Generalized Adaptive Spreading Modulation: A Novel Waveform for Integrated Sensing and Communication Oriented Vehicular Applications

Daljeet Singh, *Member, IEEE*, Atul Kumar, *Member, IEEE*, Hem Dutt Joshi, *Member, IEEE*, Ashutosh Kumar Singh, Waqar Anwar, Teemu Myllylä, Maurizio Magarini, *Member, IEEE*, Lewis Nkenyereye, *Senior Member, IEEE*, and Kapal Dev, *Senior Member, IEEE*

***Abstract*—This study aims to present a comparative analysis of existing waveforms for integrated sensing and communication (ISAC) in vehicular environments. A novel multicarrier framework called generalized adaptive spreading modulation (GASM) is proposed for ISAC-enabled vehicular environments. The GASM waveform offers symbol spreading in both time and frequency domains with tunable spreading parameters, which allows the proposed GASM-based waveform to adapt according to the rapid time-frequency variations of the fading channel. This helps to combat the most common system impairments, such as carrier frequency offset (CFO) and symbol timing offset (STO). The GASM scheme is the generalization of various existing waveforms, such as orthogonal frequency-division multiplexing (OFDM), fractional Fourier transform-based OFDM (FrFT-based OFDM), and orthogonal chirp division multiplexing (OCDM). The proposed GASM-based ISAC system is evaluated in terms of average bit error rate (ABER) for the communication and ambiguity function (AF) for sensing capabilities. The performance of the GASM-based ISAC system is found superior as compared to the existing waveforms, i.e., OFDM, FrFT-based OFDM, OCDM, generalized frequency division multiplexing (GFDM), and orthogonal time frequency space (OTFS) modulation.**

***Index Terms*—Error rate analysis, fading, integrated communication and sensing (ISAC), joint communication and radar sensing, multicarrier modulation, performance tradeoff, waveform design.**

Manuscript received 23 May 2024; revised 19 June 2024 and 2 July 2024; accepted 14 July 2024. Date of publication 18 July 2024; date of current version 6 September 2024. This work was supported in part by the Global Pilots financed by the Finnish Ministry of Education and Culture as part of the Project INDFICORE; in part by the European Union (EU) for Erasmus+KA171; and in part by the 6GBRIDGE—Next Generation Healthcare and Wearable Diagnostics Utilizing 6G under Grant 11146/31/2022. *(Corresponding authors: Daljeet Singh; Lewis Nkenyereye.)*

Daljeet Singh is with the Research Unit of Health Sciences and Technology, University of Oulu, 90570 Oulu, Finland, and also with the Division of Research and Development, Lovely Professional University, Phagwara 144411, India (e-mail: daljeetsingh.thapar@gmail.com).

Atul Kumar is with the Department of Electronics Engineering, Indian Institute of Technology (BHU) Varanasi, Varanasi 221005, India (e-mail: atul.ece@iitbhu.ac.in).

Hem Dutt Joshi and Ashutosh Kumar Singh are with the Department of Electronics and Communication Engineering, Thapar Institute of Engineering and Technology, Patiala 147001, India (e-mail: hemdutt.joshi@thapar.edu; aksingh@thapar.edu).

Waqar Anwar is with the Vodafone Chair Mobile Communications Systems, Technical University of Dresden, 01069 Dresden, Germany (e-mail: waqar.anwar@tu-dresden.de).

Teemu Myllylä is with the Research Unit of Health Sciences and Technology, University of Oulu, 90570 Oulu, Finland (e-mail: eemu.myllyla@oulu.fi).

Maurizio Magarini is with the Dipartimento di Elettronica, Informazione e Bioingegneria, Politecnico di Milano, 20133 Milan, Italy (e-mail: maurizio.magarini@polimi.it).

Lewis Nkenyereye is with the Department of Computer and Information Security, Sejong University, Seoul 05006, South Korea (e-mail: nkenyele@sejong.ac.kr).

Kapal Dev is with the Department of Computer Science and CONNECT Centre, Munster Technological University, Bishopstown, Cork, T12 P928, Ireland, also with the Department of Institute of Intelligent Systems, University of Johannesburg, Auckland Park 2006, South Africa, and also with the Department of Electrical and Computer Engineering, Lebanese American University, Byblos 135053, Lebanon (e-mail: kapal.dev@mtu.ie).

Digital Object Identifier 10.1109/JIOT.2024.3431200

I. ISAC for Vehicles: Motivation and User Cases

RECENT years have witnessed the rise of smart era of Internet of Everything (IoE) wherein every system is aiming to become autonomous and self-sustaining for improving the human lifestyle. This booming intelligence in technology is suffusing every sector of society resulting in Industry 4.0, smart energy, smart cities, and smart transportation. The incorporation of 6G IoE in transport infrastructure has materialized futuristic applications, such as pedestrian detection, lane change caution, traffic sign observance, emergency braking, and finally fully autonomous driving which were just a dream in the past. The incubation of autonomous driving capabilities in vehicles has proven to enhance the driving experience by reducing vehicle accidents and liberating thousands of humans from the tedious task of driving [1].

A. Motivation

The current vehicles are equipped with an advanced driver assistance system (ADAS) to make driving autonomous that harnesses the information from the onboard devices and sensors [2]. To attain level five autonomous driving with full automation in labyrinthine driving environments, the vehicles can not rely only on the sensing information from ADAS but also require supplementary support from surrounding infrastructure through communication [3]. Such advanced vehicular systems involve the integration of communication and sensing capabilities to use the same equipment, spectrum, and signals for both sensing and communication purposes. This integration improves the overall efficiency of the system in terms of

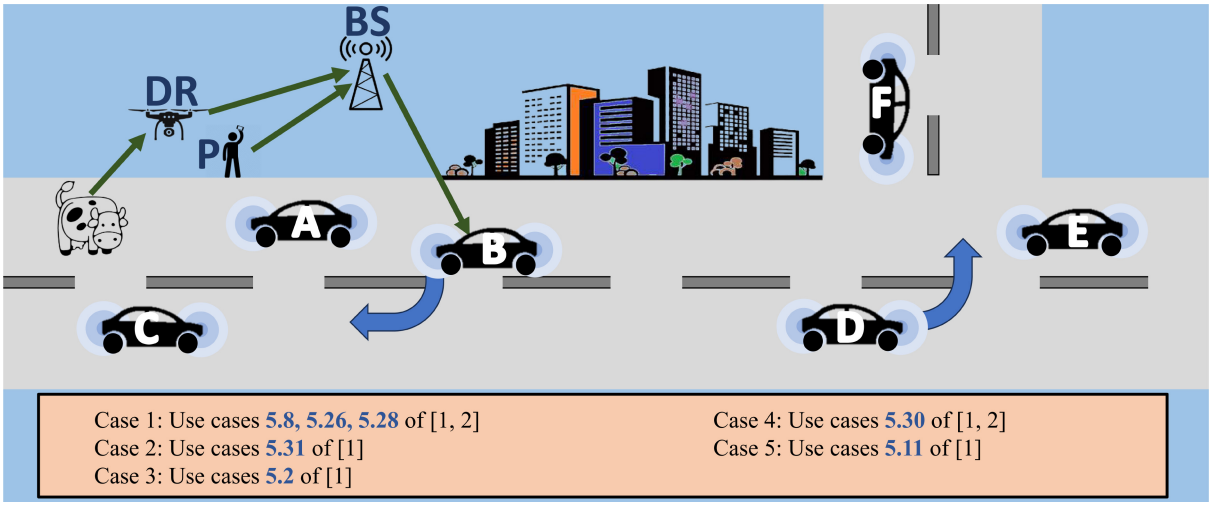

Fig. 1. Scenario replicating different use cases of the practical fully autonomous vehicular environment based on 3GPP feasibility study on ISAC in Release-19 [5] and C-V2X white paper [6].

spectral usage, hardware utilization, and information processing which motivates the recent research theme of integrated sensing and communications (ISACs) [4]. The performance of an ISAC system for sensing targets and simultaneously communicating data depends heavily on the waveform design. The traditional radar and communication waveform are not suitable for ISAC applications. A detailed analysis of this issue is presented in Section II. Therefore, the development of a novel waveform especially designed for ISAC is the need of the hour to realize practical ISAC applications.

B. Use Cases of ISAC in Vehicular Environments

An ISAC-oriented vehicular environment in 6G IoE includes interactions between the vehicle-to-vehicle (V2V), vehicle-to-pedestrian (V2P), and vehicle-to-infrastructure (V2I) for safe and efficient transportation. Several use cases and system key performance indicators (KPIs) required for these vehicular interactions involving ISAC have been presented recently in cellular-vehicle-to-everything (C-V2X) white paper by 5G automotive association [6] and 3rd generation partnership project (3GPP) feasibility study on the ISAC in Release-19 [5]. Some of the relevant use cases with original terminology and serial number are: 5.2: pedestrian/animal intrusion detection on a highway, 5.7: sensing for railway intrusion detection, 5.8: sensing assisted automotive maneuvering and navigation, 5.11: sensing at crossroads with/without obstacle, 5.26: accurate sensing for automotive maneuvering and navigation service, 5.28: vehicles sensing for ADAS, 5.30: sensing for automotive maneuvering and navigation service when not served by random access network, and 5.31: blind spot detection [5].

Fig. 1 showcases a scenario generated especially to replicate the practical fully autonomous vehicular environment based on the ISAC system. Case 1 subsumes more generic use cases 5.8, 5.26, and 5.28 and other applications, such as cooperative traffic gap, infrastructure-assisted environment perception, and teleoperated driving support, wherein all the vehicles are working in autonomous mode using ADAS and assistive automotive maneuvering and navigation [6]. Case 2 is a more complex situation of blind spot detection (5.31) and vehicle decision assist in which Vehicle B is trying to overtake Vehicle A but is cautioned by A about incoming Vehicle C.

Infrastructure-assisted environment perception is visualized in Case 3 of Fig. 1 assuming that there is an animal on the road and a pedestrian (P) standing near the road which are detected by ADAS of Vehicle A but not by Vehicle B. Therefore, drone (DR) gives this sensing information to B through the base station (BS). The use case 5.30 is covered in Case 4 wherein Vehicle C cannot connect to BS or DR. Therefore, Vehicle C requests assistance in terms of sensing data from Vehicles A and B to maneuver safely through traffic [5]. Finally, in Case 5, the use case 5.11 is undertaken as Vehicle D wants to take a left turn on a crossroad but does not have enough information about its surroundings to make an educated decision. Therefore, Vehicle D requests assistance in terms of sensing data from Vehicles E and F to turn safely [5]. It should be noted that the ISAC system undertaken in this study is applicable to both the driven and autonomous vehicles and is not limited to these use cases only.

II. Review of Existing Waveforms for ISAC

The waveform design is backbone of every ISAC system wherein the choice of a particular waveform influences its overall performance. Section II-A provides an overview of the existing waveforms that have been proposed in the ISAC system till now. Further, the requirements and challenges while designing a waveform for the ISAC system are presented in Section II-B.

A. Traditional ISAC Waveforms

To date, most of the co-design ISAC systems have focused on utilizing the existing waveforms and the associated modulation schemes [7]. The joint radar-communication (JRC) system implements communication as a secondary function on a radar platform and utilizes the chirp sequence, phase-modulated continuous wave (PMCW), frequency-modulated

TABLE I
COMPARISON OF AVAILABLE WAVEFORMS WITH PROPOSED GASM IN TERMS OF SYMBOL SPREADING CAPABILITIES

Waveform	Spreading domain					Type of Spreading
	Time	Frequency	Delay	Doppler	Chirp	
OFDM	No	Yes	No	No	No	1-D Static
FrFT-based OFDM	No	Yes	No	No	No	1-D Static
DFT-s-OFDM	Yes	No	No	No	No	1-D Static
GFDM	Yes	Yes	No	No	No	2-D Static
OTFS	No	No	Yes	Yes	No	2-D Static
OCDM	Yes	No	No	No	Yes	2-D Static
Proposed GASM	Yes	Yes	No	No	No	2-D Adaptive

continuous-wave (FMCW), and its variations [8]. This JRC system achieves satisfactory sensing performance but fails to accomplish the goal of high data rate communication which is not suitable for the real-time vehicular applications.

On the other hand, the joint communications-radar (JCR) system, implements the secondary radar functions on a standardized communication system by utilizing the digital multicarrier schemes, such as orthogonal frequency-division multiplexing (OFDM), fractional Fourier transform-based OFDM (FrFT-based OFDM), generalized frequency division multiplexing (GFDM), discrete Fourier transform-spread-OFDM (DFT-s-OFDM), orthogonal chirp division multiplexing (OCDM), orthogonal time frequency space (OTFS), etc., thus achieving decent communication performance but sacrificing the sensing [9]. Therefore, there is a very strong motivation to design a novel unified waveform that does not favor one or the other by default but rather adapts according to the application requirements.

B. Challenges in Designing ISAC Waveform

There are two main challenges while designing a waveform for an ISAC-based vehicular system, which are hereafter discussed as follows.

1) Tunable Parameters for Communication Sensing Tradeoff: The first challenge is the tradeoff between the communication and sensing performance of the ISAC systems. The reason behind this is that even though the radar and communication systems work on the similar frequencies, they differ completely in waveform design due to the unique KPIs [7]. Moreover, both the systems operate under different channel conditions and have different time-frequency characteristics of the signal. Therefore, the ISAC system should have tunable parameters to optimize the radar and communication performance to fulfill the Quality of Service (QoS) requirements.

2) Catering Fading and System Impairments: Another key requirement for the ISAC systems is that the designed waveform should suit the rapidly varying dual time-frequency selective (TFS) fading scenarios. Furthermore, the designed ISAC waveform should be robust to the Doppler shifts in typical high-frequency bands suggested for most of the ISAC applications in 6G. Table I evaluates the available waveforms with proposed generalized adaptive spreading modulation (GASM) in terms of symbol spreading capabilities and type of spreading. It is clearly evident from Table I that OFDM, FrFT-based OFDM, and DFT-s-OFDM can only achieve static spreading in either time or frequency domains [10]. Therefore, these waveforms can perform optimally in only either time-selective or frequency-selective channels.

A higher diversity gain can be realized by achieving symbol spacing in two dimensions, resulting in improved system performance [10]. This is evident from the popularity of GFDM, OTFS, and OCDM systems that achieve 2-D symbol spacing. However, none of these waveforms offers 2-D adaptive spreading in the time-frequency domain, which can be optimized as per the system requirements and channel conditions. The flexible numerology outlined in recent standards of ETSI/3GPP for 5G NR (new radio) suggests a dynamic model for choosing the subcarrier spacing in frequency based on the channel conditions. The proposed GASM approach not only supports the dynamic models of choosing subcarrier spacing in frequency domain based on the channel conditions (which gives 1-D dynamic spreading) but also offers the symbol spreading in the time domain and therefore can achieve 2-D dynamic spreading with adaptive spacing parameters.

III. ISAC ARCHITECTURE IN VEHICULAR ENVIRONMENT

The system model of the ISAC in a vehicular environment is presented in Fig. 2. Referring to the fully autonomous vehicular environment shown in Fig. 1, all the vehicles are assumed to be equipped with an ISAC module capable of performing two tasks simultaneously, i.e., 1) communicating the data available with the current ISAC module to those of the other vehicles and 2) sensing the targets near vehicle by processing the reflections of the transmitted signal from the multiple targets. For simplification, we have considered the ISAC module in in-band full-duplex (IBFD) mode working with single-input–single-output (SISO) configuration.[1]

The following sections describe the assumptions undertaken while making the system, transmitter, and receiver models of the ISAC system undertaken in this work.

A. Assumptions

1) The ISAC nodes of the system are assumed to be operating in the IBFD mode.
2) The transmitting and receiving antennas at the ISAC nodes are in quasi-colocation (QCL) of type A (QCL-A).
3) The change in the channel between the transmitter and receiver ISAC as well as the transmitter ISAC and targets is induced by only Doppler shift.

[1]The analysis presented here can be easily extended to include any number of ISAC modules with multiple-input–multiple-output (MIMO) configuration.

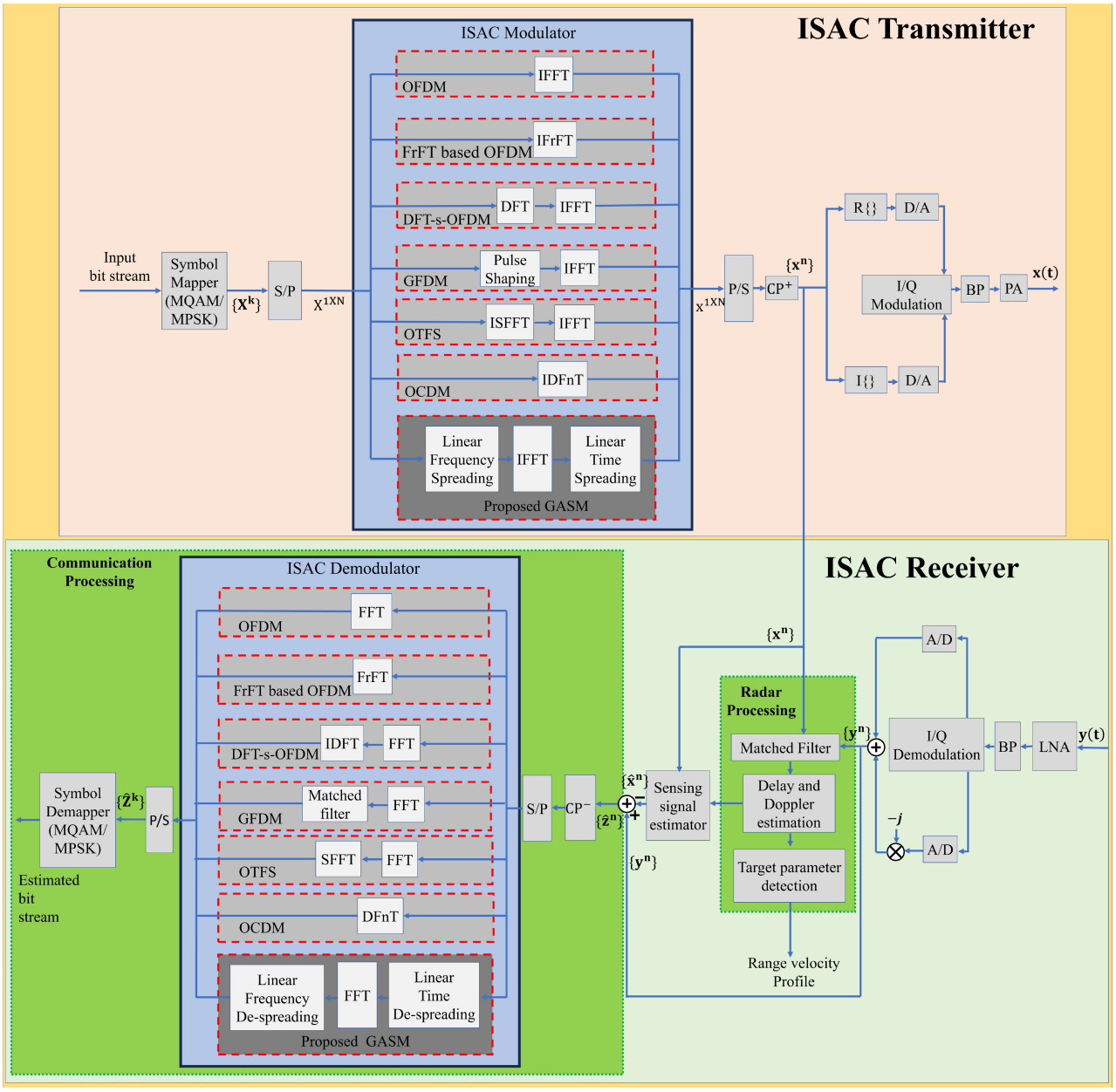

Fig. 2. Detailed block diagram of ISAC system.

These assumptions are not compulsory but are very straightforward and hold true for most vehicular environments. The analysis presented in the manuscript can be applied to any type of transmission, including IBFD. The generic case of IBFD is considered here as it offers optimized system performance. However, the IBFD system suffers from self-interference and requires precisely designed interference cancelation techniques. Moreover, the performance of the proposed waveform is independent of these assumptions.

B. Transmitter Model

The detailed block diagram depicting the transmitter of an ISAC module is given in Fig. 2. The transmitted signal consists of F frames each of duration t_F. Each frame consists of B data blocks of duration t_B. Each data block consists of one ISAC symbol carrying N complex data symbols, and G cyclic prefix (CP) symbols. For the generation of one ISAC symbol, the input bit stream is first converted into complex data symbols $\{\mathbf{X}^k\}$ using either the M-QAM or M-PSK modulation scheme. Then, these serial complex data symbols are converted into N parallel complex data symbols using a serial-to-parallel converter (S/P). These N parallel symbols are then processed using the ISAC modulator. In order to present a comparative analysis of existing waveforms for ISAC, the ISAC modulator is divided into sub-blocks each representing an unique waveform-specific transmitter for OFDM, FrFT-based OFDM, DFT-s-OFDM, GFDM, OTFS, OCDM, and proposed GASM. The N parallel symbols are fed to any one of the sub-blocks depending on the chosen waveform design. The output of ISAC modulator is then converted into serially arranged ISAC symbols $\{\mathbf{x}^n\}$ using a

parallel-to-serial converter (P/S). Thereafter, the CP of length G is added to each ISAC symbol, which generates a data block of size $N+G$. The transmitted signal before bandpass modulation can be represented as

$$\{\mathbf{x}^n\} = \mathrm{CP}_G^+\Big[\wp\Big[\{\mathbf{X}^k\}\Big]\Big] \tag{1}$$

where $\wp$ denotes the waveform-specific ISAC modulator as shown in the transmitter model of Fig. 2 and CP_G^+ represents the operation of CP addition of length G. Finally, the data block containing the baseband ISAC samples $\{\mathbf{x}^n\}$ is converted into a bandpass equivalent using a digital-to-analog converter (DAC) and I/Q modulation.

C. Receiver Model

At the receiver side, the received bandpass signal $y(t)$ is processed by the radar processing block, which estimates the range velocity profile of the target, and communication processing block, which extracts modulated data transmitted by the other ISAC modules. The received signal $y(t)$ is represented mathematically as

$$\begin{aligned} y(t) = &\sum_{h=0}^{H-1} \alpha_h x(t-\tau_h)\exp\left(j2\pi f_h^D t\right) \\ &+ \sum_{p=0}^{P-1} \alpha_p z\left(t-\tau_p-\delta_t\right)\exp\Big(j2\pi f_p^D t\Big)\exp\left(j2\pi\delta_f t\right) \\ &+ w(t) \end{aligned} \tag{2}$$

where the first term represents the echo of the signal transmitted from the ISAC module of the current vehicle ($x(t)$), which is reflected off by a total of H radar targets, labeled as $h \in \{0,1,\ldots,H-1\}$, and received by same ISAC module. Further, α_h represents the attenuation faced by reflected signal in traveling to and fro from hth target; which depends upon the carrier frequency, radar cross section, and gain of the ISAC antenna. The delay and Doppler shift suffered radar reflections from hth target are denoted by τ_h and f_h^D, respectively. The second term in (2) accounts for the communication signal transmitted from the ISAC module of the other vehicle ($z(t)$) which propagates through P multipath in the medium, labeled as $p \in \{0,1,\ldots,P-1\}$. Similar to the first term, α_p, τ_p, and f_p^D represent the attenuation, delay, and Doppler shift, respectively, which is faced by communication signal while traveling from pth path. Further, δ_t and δ_f represent the system impairments symbol timing offset (STO) and carrier frequency offset (CFO), respectively. The third term $w(t)$ denotes the additive white Gaussian noise (AWGN). The received signal $y(t)$ is first converted into its baseband equivalent using a low noise amplifier (LNA), band pass filter, and I/Q demodulator. After this, the baseband signal $\{\mathbf{y}^n\}$ is processed by the radar processing block to generate the range velocity profile of the targets.

As shown in Fig. 2, the radar processing starts by feeding $\{\mathbf{y}^n\}$ and transmitted ISAC data block $\{\mathbf{x}^n\}$ to the matched filter. The output of the matched filter block is then given to the delay and Doppler estimation block that calculates the Doppler spread and time delay of the received signal with respect to the transmitted signal. This delay and Doppler information are further utilized by the target parameter detection block to generate the range velocity profile of the targets. The group of these three blocks, i.e., matched filter, delay-Doppler estimation, and target parameter detection blocks are collectively termed as the radar processing block.

Next, an estimated radar signal, $\hat{x}^n$, is calculated using the sensing signal estimator block as

$$\{\hat{x}^n\} = x^{n-\hat{\tau}_h^n}\exp\left(j2\pi\hat{f}_h^D[n]\right) \tag{3}$$

where $\hat{\tau}_h^n$ and $\hat{f}_h^D[n]$ is the estimated delay and Doppler shift calculated by the delay and doppler estimation block. Further, an estimated communication signal, $\{\hat{z}^n\}$, is derived by extracting $\{\hat{x}^n\}$ from the overall received signal $\{y^n\}$. After this, the CP is removed from $\{\hat{z}^n\}$ and is fed to the S/P convertor. The output of the S/P converter is then given to the ISAC demodulator that consists of waveform-specific receivers. The output of the ISAC demodulator is then converted into serially arranged estimated communication symbols $\{\hat{\mathbf{Z}}^k\}$ using a P/S converter. These estimated communication symbols are finally converted into an estimated bit stream using a suitable demodulation scheme.

IV. Novel Waveform Design for ISAC System

Motivated by the challenges and requirements listed in Section II-B, and the ISAC system described in Section III, a novel waveform design is presented in this section whose synthesis is shown in Fig. 2. The novel waveform design is named GASM and has the ability to control the symbol spreading in both time as well as frequency domains independently. First, the complex data symbols generated using a typical modulation scheme (M-QAM/M-PSK) are passed through the linear frequency spreading. These linear frequency-modulated signals are then transformed into the time domain using the inverse fast Fourier transform (IFFT). Next, these symbols are processed by linear time spreading that results in further spreading of the signal in the time domain and gives samples of the proposed GASM waveform.

The process of generating the proposed GASM waveform can be mathematically expressed as

$$X[m] = \frac{1}{\sqrt{N}} \overbrace{\exp\left(j\sigma_t m^2\Delta_f^2\right)}^{\text{linear frequency spreading}} \sum_{n=-\infty}^{\infty} x[n] \overbrace{\exp\left(j\sigma_f n^2\Delta_t^2\right)}^{\text{linear time spreading}} \exp\left(j2\pi\frac{mn}{N}\right) \tag{4}$$

where $\Delta_t = (1/f_{\text{sample}})$ is the sampling interval in the time domain, f_{sample} is the sampling frequency, and the parameters σ_t and Δ_f are the time spreading factor and sampling interval of the resultant signal, respectively. The sampling interval of the resultant signal is calculated as $\Delta_f = (2\pi c/N\Delta_t)$ by using the generalized sampling theorem relating sampling frequency with σ_t and σ_f as [11], with the constant c as the highest common factor that can divide σ_t and σ_f.

The inclusion of quadratic terms in (4) implies a departure from the equidistant subcarrier spacing characteristic of classical OFDM, FrFT-based OFDM, DFT-s-OFDM, and GFDM.

Algorithm 1 Optimization Algorithm for Calculation of Optimal Waveform Parameters for ISAC

INITIALIZATION
Initialize parameters: $\sigma_t = \sigma_{t_0}$, $\sigma_f = \sigma_{f_0}$, $Step_t$, $Step_f$, $\gamma_{lopt} = []$
LEARNING
for $i = 1$ to I **do**
for $k = 1$ to K **do**
Calculate $\gamma_{lopt}(i,k)\Big|_{\sigma_{t_i},\sigma_{f_k}}$ $\forall$ channel instance Ψ
Update $\sigma_f = \sigma_f + Step_f$,
end for
Update $\sigma_t = \sigma_t + Step_t$,
end for
UPDATE OPTIMUM PARAMETERS
$\gamma_{opt} = \max[\gamma_{lopt}(i,k)]$ $\forall$ channel instance Ψ
$[\sigma_{topt}, \sigma_{fopt}] = ind[\max[\gamma_{lopt}(i,k)]]$ $\forall$ channel instance Ψ

It should be noted that these conventional techniques do not offer such adaptive spreading parameters and therefore can achieve only static spreading in only one or two dimensions as denoted in Table I. The availability of 2-D adaptive spreading contributes to the improved performance of the proposed GASM approach which is visualized by numerous simulation results for performance comparison presented in Section VII.

V. Proposed Optimization Algorithm for GASM Parameters

The proposed GASM-based ISAC waveform can be optimized in terms of σ_t and σ_f as given in (4) to achieve the optimum symbol spacing Δ_t and Δ_f in both the time and frequency domains to best suit the system KPI requirements for a given set of the system parameters, channel conditions, and impairments. This optimization problem aims to maximize the instantaneous signal-to-interference-plus-noise ratio (SINR) γ at a given channel instance Ψ, which ultimately affects both the sensing and communication capabilities of the system.

The algorithm devised for calculating the optimal parameters of GASM for the ISAC applications is presented as Algorithm 1. In the initialization phase, the system parameters are defined $\sigma_t = \sigma_{t_0}$, $\sigma_f = \sigma_{f_0}$, Step_t, and Step_f, where σ_{t_0} and σ_{f_0} are the initial spreading factors with step sizes Step_t and Step_f, respectively. The algorithm iterates for each channel instance Ψ and calculates the localized optimal SINR $\gamma_{lopt}(i,k)$ for the given value of $\sigma_t = \sigma_{t_i}$ and $\sigma_f = \sigma_{f_k}$. Finally, the optimized SINR is calculated as maxima of $\gamma_{lopt}(i,k)$. The corresponding optimal waveform parameters σ_{topt} and σ_{fopt} are chosen as the final parameters to achieve the best possible system performance.

VI. Special Cases of Proposed GASM Waveform

The special cases of the proposed GASM waveform are presented in this section.

A. OFDM

With careful observation of (4), it can be observed that the proposed ISAC waveform can be converted into OFDM by substituting $\sigma_t = \sigma_f = 0$.

TABLE II
Simulation Parameters for Performance Comparison

Parameter	value
System parameters	
MCS	GASM, OFDM,GFDM, OTFS, FrFT based OFDM, OCDM
FFT length	64, GFDM(16,4)
Modulation order	2
Modulation	PSK
Channel Equalization	Zero forcing
Symbol duration	6.4 μs
Cyclic prefix	1.6 μs
Transmission power	0 dBm
Radar maximum unambiguous range	LRR: 300m and SRR: 100m
Radar range resolution	LRR: 75cm and SRR: 20cm
Target velocity	LRR: 50 m/s and SRR: 30m/s
Velocity resolution	LRR: 0.1m/s and SRR: 0.1m/s
Latency	LRR: 50 ms and SRR: 20ms
Missed detection	LRR: 1-10% and SRR: 1-10%
False alarm	LRR: $<$1% and SRR: $<$1%
Channel parameters	
Channel bandwidth	10 MHz
Maximum doppler shift	150 Hz (FSF), 2000 Hz (TFS)
Channel taps	4
Relative power of each tap	[0, -10, -14, -18] dB
Excess delay of each tap	[0, 0.4, 0.7, 1] μs
Fading distribution	Rayleigh

B. FrFT-Based OFDM

The FrFT-based OFDM can be implemented from the proposed GASM by substituting $\sigma_t = \sigma_f = \cot(\phi)$.

C. OCDM

The OCDM can also be implemented as a special case of the proposed waveform by substituting $\sigma_t = \sigma_f = \Phi$ (constant similar to the chirp rate). Now, it is clear that OFDM, FrFT-based OFDM, and OCDM are the special cases of the proposed waveform, and therefore the values of σ_t and σ_f can be suitably tuned to replicate the performance of these MCSs.

VII. Performance Comparison

In this section, the performance analysis of the proposed GASM-based ISAC system is presented and compared with other standard MCSs: OFDM, FrFT-based OFDM, GFDM, OTFS, and OCDM. The system parameters utilized for performance analysis are given in Table II. These system parameters are inspired by the use cases and service level requirements presented in C-V2X white paper [6] and 3GPP feasibility study on ISAC in Release-19 [5].

In order for the results to be coherently analysed and to ensure fair comparison, the ISAC system considered in the simulations utilizes uniform energy and bit allocation techniques. Moreover, keeping in mind the practical constraints regarding signal processing, the signals are processed in the time-frequency domain and the zero forcing channel equalization method is utilized at the receiver [12]. The communication performance of the proposed ISAC system is evaluated in Section VII-A, wherein the average bit error rate (ABER) experienced by the system is calculated. The sensing performance of the ISAC system is evaluated based on the well-known ambiguity function (AF) approach in Section VII-B.

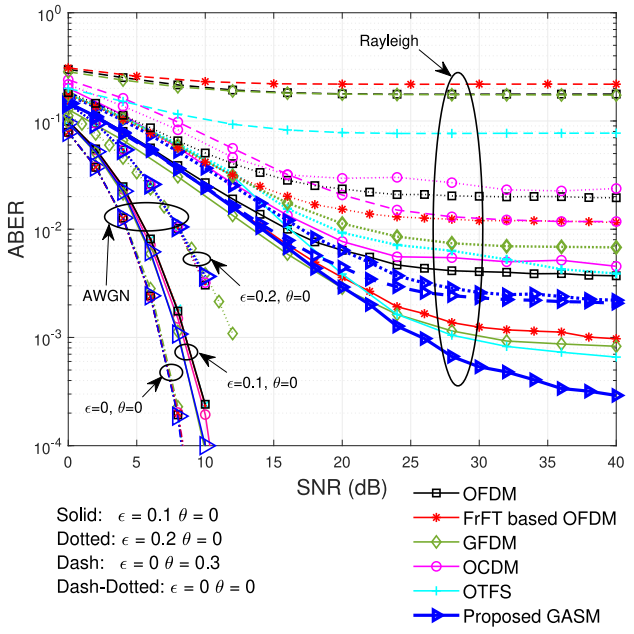

Fig. 3. ABER v/s SNR plot of proposed GASM-based ISAC system with existing MCSs over AWGN and frequency-selective Rayleigh fading channel with two-taps equal power delay profile.

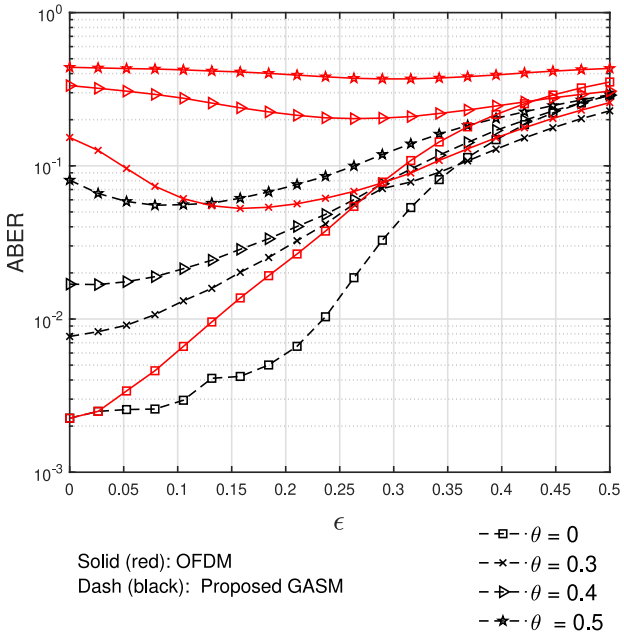

Fig. 4. ABER v/s ϵ plot of proposed GASM-based ISAC system with OFDM over frequency-selective Rayleigh fading channel at SNR = 20 dB.

A. Communication Performance

As per the requirements listed in [5] and [6], a data rate of 300–1400 bytes per message for the periodic kinematics and position information and 8–35 MB/s for camera and Lidar streaming is required which is fulfilled by all the MCS listed in Table II. The ABER performance of the ISAC system is evaluated under AWGN, frequency selective fading (FSF), and TFS or doubly selective fading channels with CFO and STO. The CFO normalized to subcarrier spacing is denoted by ϵ, whereas the normalized STO is denoted by θ. Fig. 3 shows the ABER v/s SNR plot for the proposed GASM-based ISAC system under perfect synchronization ($\epsilon = 0$ and $\theta = 0$), with only CFO ($\epsilon = 0.1$ and $\theta = 0$), ($\epsilon = 0.2$ and $\theta = 0$), and with STO ($\epsilon = 0$ and $\theta = 0.3$) cases over AWGN and frequency-selective Rayleigh fading channel with two-taps equal power delay profile channel. It can be visualized from Fig. 3 that the ABER performance of the proposed GASM-based ISAC system matches with the other state-of-the-art MCSs, i.e., OFDM, FrFT-based OFDM [13], GFDM [14], and OCDM [12] in AWGN. This justifies that the GASM performs at par when compared with the standard modulation schemes under the AWGN channel conditions.

However, this trend does not hold under a more challenging FSF scenario, wherein the proposed GASM scheme outperforms all the other MCSs due to its superior capability to handle fading variations and synchronization errors. It is clearly observed from Fig. 3 that the ABER performance of GASM is better than the other standard MCSs [13], [14], [15], especially in the practical SNR range. For example, at fixed SNR = 30 dB, the ABER of GASM, OFDM, FrFT-based OFDM, GFDM, and OCDM are 5.35×10^{-4}, 4.05×10^{-3}, 1.24×10^{-3}, 1.04×10^{-3}, and 5.21×10^{-3}, respectively.

In order to study the effect of CFO and STO in more detail, the ABER of the proposed system is calculated for $\epsilon = [0 - 5]$ with different values of $\theta = 0, 0.3, 0.4,$ and 0.5 at a constant SNR of 20 dB in Fig. 4. It can be observed from Fig. 4 that in all the presented cases, the performance of GASM is better than the OFDM system [13]. An interesting observation from Fig. 4 is that the performance of OFDM is very poor and reaches an error floor when the system is exposed to high timing offset errors ($\theta = 0.3, 0.4, 0.5$), etc. but the performance of the GASM-based ISAC system is satisfactorily much better [13]. Therefore, the resilience of the proposed GASM scheme against impairments is evident under the complex practical scenarios from Fig. 4.

B. Radar Performance

This section presents the sensing performance of the ISAC system with the proposed scheme and its comparison with the other standard MCSs. For this purpose, the AF of the ISAC waveform is evaluated to study its range and Doppler capabilities. The results are calculated for the long-range radar (LRR) and short-range radar (SRR) scenarios depicted in Table II. Fig. 5 presents the AF v/s Doppler plots with zero delay shift in LRR environment for the BPSK modulated GASM data and compared with the other MCSs. It is well known that the presence of dominant side lobes affects the sensing performance of radar. This results in a decreased probability of detection and higher false alarm rates, especially with higher Doppler shifts associated with relative radial velocities of targets, and can be computed numerically as the mean side lobe level (μ).

It can be visualized from Fig. 5 that the AF curve of the proposed GASM-based waveform has lower side lobe levels as compared to the other MCSs. The mean side lobe level of AF v/s Doppler ($\mu_{doppler}$) for proposed GASM is only 0.122 while for OFDM, FrFT-based OFDM, GFDM, OTFS, and OCDM are 0.1873, 0.1852, 0.3713, 0.2383, and 0.2962, respectively,

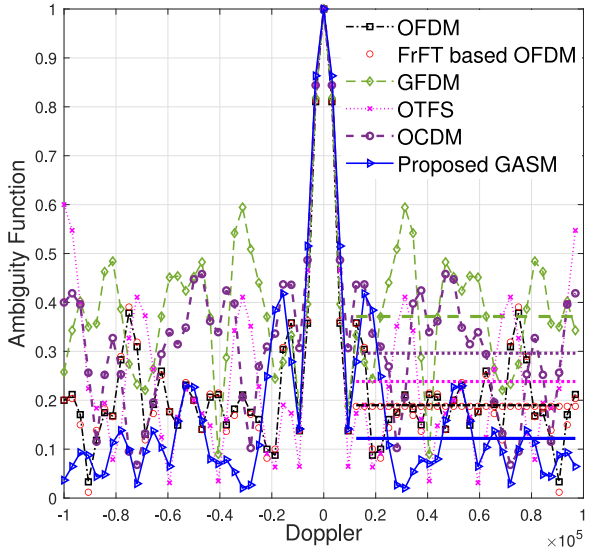

Fig. 5. AF v/s delay of proposed GASM-based ISAC system with existing MCSs with zero Doppler shift.

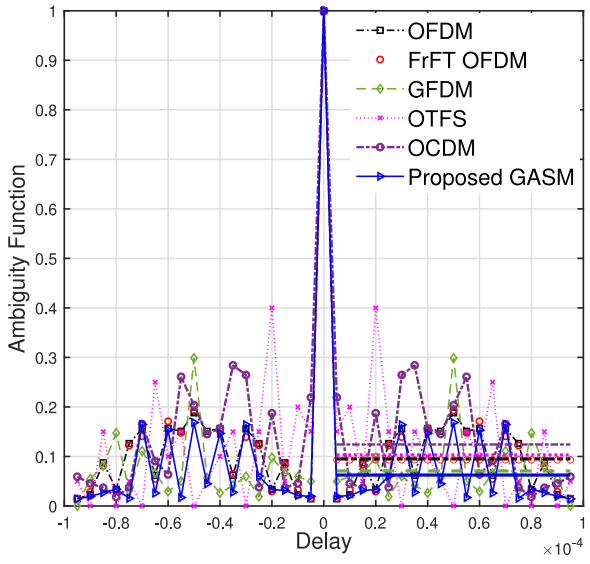

Fig. 6. AF v/s Doppler of proposed GASM-based ISAC system with existing MCSs with zero delay shift.

thus achieving a percentage improvement of 53.52, 51.80, 204.34, 95.32, and 142.78 percent, respectively; as compared with the other MCSs. Further, the corresponding plot of AF v/s delay with zero Doppler shift in LRR environment for the BPSK modulated GASM data is shown in Fig. 6. A trend similar to Fig. 5 is also visible in Fig. 6 wherein the proposed GASM-based waveform shows the sharpest main lobe with minimum mean side lobe level (μ_{delay}). The value of (μ_{delay}) for proposed GASM is only 0.0625 while for OFDM, FrFT-based OFDM, GFDM, OTFS, and OCDM are 0.1873, 0.1852, 03713, 0.2383, and 0.2962.

VIII. Conclusion

In this article, a novel multicarrier framework based on GASM is proposed and analysed for the ISAC-based vehicular systems. The standard MCSs, such as OFDM, FrFT-based OFDM, and OCDM are derived as special cases of the proposed GASM. The proposed GASM-based ISAC system is evaluated for both communication and sensing performance in fading channels with CFO and STO. It is observed from the simulation results that the proposed GASM-based ISAC system has superior performance in terms of ABER under TFS fading environments under the effect of synchronization errors. On a similar note, the proposed GASM system sensing showcases better sensing performance in terms of range and Doppler calculation from AF of the transmitted waveform. The ability to fine tune the symbol spreading in both time and frequency domains to best suit the fading scenario is the prime reason for such superior performance of GASM.

Acknowledgment

The authors thank INDFICORE (India-Finland cooperation on 6G) under the 6G Flagship group at the University of Oulu, Finland; Erasmus+Program (Erasmus+KA171) with Politecnico di Milano, Italy; and 5G Use Case Lab, IIT BHU, and TIET Patiala funded by Department of Telecommunication (DoT) Government of India) for providing valuable discussions. The authors alone are responsible for the content of this article.

References

[1] L. Chen, F. Liu, W. Wang, and C. Masouros, "Joint radar-communication transmission: A generalized Pareto optimization framework," *IEEE Trans. Signal Process.*, vol. 69, pp. 2752–2765, May 2021.
[2] S. Hegde, D. Plöger, R. Shrivastava, O. Blume, and A. Timm-Giel, "High-density platooning in cellular vehicle-to-everything systems: On the importance of communication-aware networked control design," *IEEE Veh. Technol. Mag.*, vol. 16, no. 3, pp. 66–74, Sep. 2021.
[3] Z. Hu, Y. Zhang, Y. Xing, Y. Zhao, D. Cao, and C. Lv, "Toward human-centered automated driving: A novel spatiotemporal vision transformer-enabled head tracker," *IEEE Veh. Technol. Mag.*, vol. 17, no. 4, pp. 57–64, Dec. 2022.
[4] Y. Zhong et al., "Empowering the V2X network by integrated sensing and communications: Background, design, advances, and opportunities," *IEEE Netw.*, vol. 36, no. 4, pp. 54–60, Jul./Aug. 2022.
[5] "Feasibility study on integrated sensing and communication," 3GPP, Sophia Antipolis, France, Rep. TR 22.837, 2023.
[6] "C-V2X use cases and service level requirements-volume III," 5GAA.org., Munich, Germany, White Paper, 2023. [Online]. Available: https://5gaa.org/content/uploads/2023/01/5gaa-tr-c-v2x-use-cases-and-service-level-requirements-vol-iii.pdf
[7] L. G. de Oliveira, B. Nuss, M. B. Alabd, A. Diewald, M. Pauli, and T. Zwick, "Joint radar-communication systems: Modulation schemes and system design," *IEEE Trans. Microw. Theory Tech.*, vol. 70, no. 3, pp. 1521–1551, Mar. 2022.
[8] G. N. Saddik, R. S. Singh, and E. R. Brown, "Ultra-wideband multifunctional communications/radar system," *IEEE Trans. Microw. Theory Tech.*, vol. 55, no. 7, pp. 1431–1437, Jul. 2007.
[9] B. J. Donnet and I. D. Longstaff, "Combining MIMO radar with OFDM communications," in *Proc. Eur. radar Conf.*, 2006, pp. 37–40.
[10] R. Bomfin, D. Zhang, M. Matthé, and G. Fettweis, "A theoretical framework for optimizing multicarrier systems under time and/or frequency-selective channels," *IEEE Commun. Lett.*, vol. 22, no. 11, pp. 2394–2397, Nov. 2018.
[11] F. Gori, "Fresnel transform and sampling theorem," *Opt. Commun.*, vol. 39, no. 5, pp. 293–297, 1981.
[12] L. de MBA Dib, G. R. Colen, M. De L. Filomeno, and M. V. Ribeiro, "Orthogonal chirp division multiplexing for baseband data communication systems," *IEEE Syst. J.*, vol. 14, no. 2, pp. 2164–2174, Jun. 2020.
[13] A. Kumar and M. Magarini, "Symbol error probability analysis of DFrFT-based OFDM systems with CFO and STO in frequency selective rayleigh fading channels," *IEEE Trans. Veh. Technol.*, vol. 68, no. 1, pp. 64–81, Jan. 2019.
[14] N. Michailow et al., "Generalized frequency division multiplexing for 5th generation cellular networks," *IEEE Trans. Commun.*, vol. 62, no. 9, pp. 3045–3061, Sep. 2014.
[15] W. Anwar, A. Kumar, N. Franchi, and G. Fettweis, "Physical layer performance modeling of modern multicarrier modulation techniques," *IEEE Trans. Commun.*, vol. 70, no. 6, pp. 3725–3741, Jun. 2022.